Nonlocal electrodynamics of long ultra-narrow Josephson junctions: Experiment and theory

A. A. Abdumalikov Jr.[†],[*] V. V. Kurin[‡], C. Helm[§], A. De Col[§], Y. Koval[†], and A. V. Ustinov[†]

[†]*Physikalisches Institut III, Universität Erlangen-Nürnberg, Erlangen D-91058, Germany*

[‡]*Institute for Physics of Microstructure (RAS), Nizhniy Novgorod, Russia*

[§]*Institut für Theoretische Physik, ETH Hönggerberg, Zürich 8093, Switzerland*

(Dated: February 2, 2008)

Abstract

We experimentally and theoretically investigate electromagnetic cavity modes in ultra-narrow Al-AlO_x-Al and Nb-AlO_x-Nb long Josephson junctions. Experiments show that the voltage spacing between the Fiske steps on the current-voltage characteristics of sub-μm wide and several hundred μm long Al-AlO_x-Al and Nb-AlO_x-Nb Josephson junctions increases when decreasing the width of a junction. This effect is explained by stray magnetic fields, which become important for narrow junctions. Theoretical estimates of the Fiske step voltage based on a nonlocal wave propagation equation are in good agreement with our experimental data. Using the nonlocal model, we determine the size and mass of a Josephson vortex by means of a variational approach, and relate vortex size to the experimentally measured critical magnetic field of the junction.

PACS numbers: 74.50.+r; 85.25.Cp; 75.70.-i

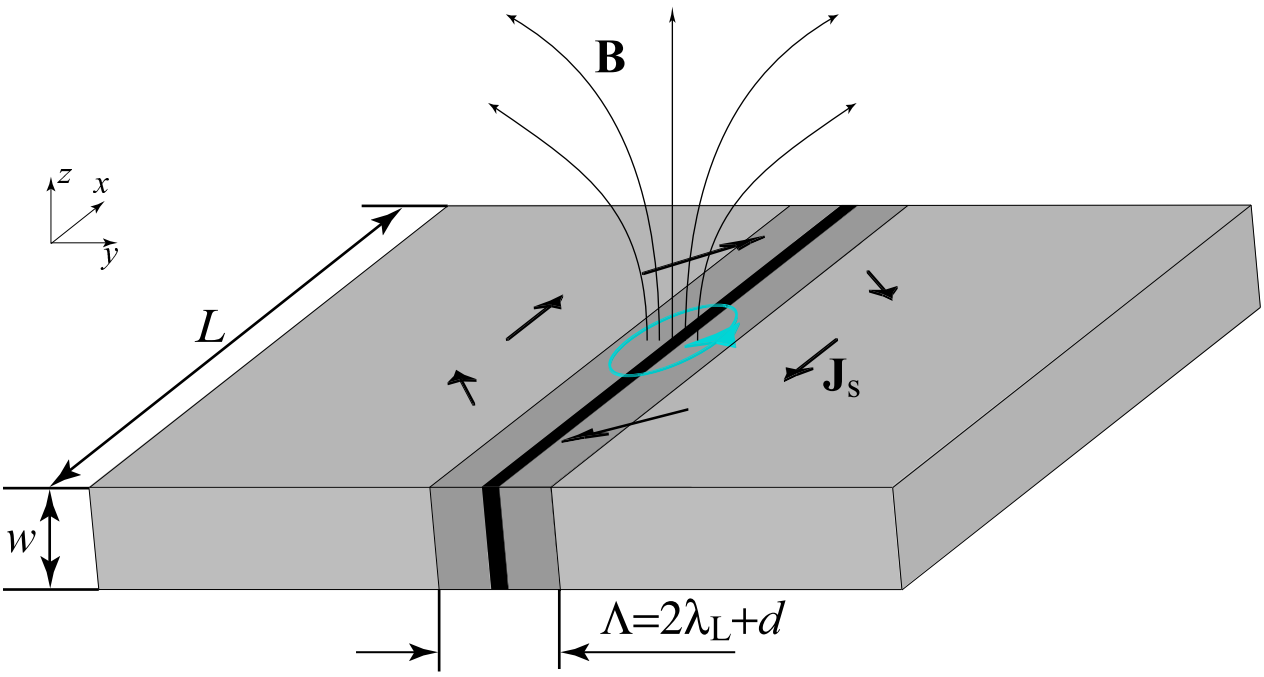

FIG. 1: Schematic view of an edge-type long Josephson junction of width w and length L. The lines show the magnetic field $\mathbf{B}$, due to vortex, which penetrates the electrodes and extends into free space. The extended stray magnetic field creates the additional surface current $\mathbf{J}_S$.

I. INTRODUCTION

The electromagnetic properties of long Josephson tunnel junctions have been the subject of intensive studies over the past four decades[1,2,3,4]. Most investigations of junction dynamics have been based on local theory. This theory assumes that electromagnetic fields are concentrated in the junction barrier, and neglects the distribution of the magnetic and electric fields outside the junction. However, in reality the fields penetrate the superconducting electrodes and extend into free space (Fig. 1). Local theory breaks down when the fields outside the junction contribute significantly to the junction energy.

The magnetic field inside the superconducting electrodes of a Josephson junction becomes important when its characteristic decay length is of the order of (or larger then) the characteristic spatial scale of variation of the Josephson phase φ. This type of nonlocality we call *internal*, because it depends only on the field distribution inside the junction and its electrodes, and neglects extended, stray, fields outside the junction.

When the energy of stray fields becomes comparable to the energy of the field inside the

junction, one has to take stray fields into account. These stray fields generate an additional surface current $\mathbf{J}_S$, which can be represented as a functional of the magnetic field distribution inside the junction, leading to a nonlocal equation. Because these effects depend on the geometry of the junction, we call them *geometrical nonlocal* effects.

Detailed knowledge of Josephson vortex dynamics is important for understanding the magnetic flux motion and related phenomena in superconductors. In a long junction, a vortex behaves like a classical particle, which is characterized by the spatial coordinate of its center and the effective mass. The interest to experimentally verify theoretically predicted nonlocal corrections to the conventional model has been biased by recent studies of long ultra-narrow junctions where Josephson vortices behave as macroscopic quantum objects[5,6]. In very narrow junctions, the *effective dynamical mass* of the vortex is expected to be influenced by nonlocally described stray magnetic fields. Most of the theoretical papers assume, however, that the effective dynamical mass of a Josephson vortex is proportional to the width of the junction as expected in the local theory[7,8,9].

In this paper, we experimentally verify that, in very narrow long Josephson junctions, one has to indeed take into account the vortex mass correction due to the stray fields outside the junction. Significant deviations from the local theory have previously been observed in the current-voltage characteristics of long junctions of small width[10]. We systematically study these effects for different junction materials, and compare the experimental findings with the nonlocal sine-Gordon model.

A Josephson junction can be considered quasi-one-dimensional, as long as its transverse dimension, the width w in z-direction (see Fig. 1), is smaller than the Josephson penetration depth

$$\lambda_J = \sqrt{\frac{\Phi_0}{2\pi\mu_0 j_c \Lambda}}, \tag{1}$$

where Φ_0 is the magnetic flux quantum, j_c is the critical current density across the tunnel barrier, $\Lambda = 2\lambda_L + d$ is the magnetic thickness of the junction, λ_L is the London penetration depth and d is the barrier thickness (typically, $d \ll \lambda_L$). In this limit ($w \ll \lambda_J$), the long junction is described by the perturbed one-dimensional sine-Gordon equation for the Josephson phase difference φ

$$\lambda_J^2 \varphi_{xx} - \omega_p^{-2} \varphi_{tt} - \omega_p^{-1} \alpha \varphi_t - \sin\varphi = \gamma, \tag{2}$$

where subscripts mean partial derivatives with respect to the spatial coordinate x along the junction and time t. The parameter

$$\omega_p = \sqrt{\frac{2\pi j_c}{\Phi_0 C}} \tag{3}$$

is the Josephson plasma frequency, C is the specific capacitance of the junction per unit area, and α is the dissipation coefficient due to the quasiparticle tunnelling across the barrier. The bias current density $\gamma = j/j_c$ is normalized to the critical current density j_c and is, in general, dependent on x.

Equation (2) is derived using the following assumptions: i) $\lambda_L \ll w \ll \lambda_J$ and ii) $\hbar\omega \ll \Delta$, where ω is the oscillation frequency of the phase φ, and Δ is the superconducting energy gap of the electrodes. The breakdown of any of these conditions requires modification of Eq. (2). As mentioned above, for large London penetration depths $\lambda_L \geq \lambda_J$ (or small Josephson penetration depths λ_J) the magnetic field inside the superconductor starts to play an important role. On the other hand, for sufficiently small junction width $w \sim \lambda_L$, the stray fields outside the junction have to be taken into account. In either case, the dynamics of the phase φ has to be described by an integro-differential equation, i.e. the problem becomes nonlocal. When the oscillation frequency ω is comparable to the superconducting gap Δ, the frequency dependence of the London penetration depth $\lambda_L(\omega)$ according to the microscopic theory (*material dispersion*) should also be taken into account[11,12,13].

The nonlocal equation describing Josephson phase dynamics can be written in the general form

$$\lambda_J^2 \frac{\partial}{\partial x} \int dx' Q(x,x') \varphi_{x'}(x') - \omega_p^{-2} \varphi_{tt} - \omega_p^{-1} \alpha \varphi_t - \sin\varphi = \gamma, \tag{4}$$

where the function $Q(x,x')$ is the nonlocality kernel, which needs to be specifically determined for each nonlocal problem. In the local case $Q(x,x') = \delta(x-x')$, where $\delta(x)$ is a delta function. Several theoretical approaches have been proposed for different types of nonlocality, in the case of an infinitely long Josephson junction. In the limit of an infinitely long junction, the kernel of the integral in Eq. (4) is reduced to the function of a single argument, $Q(x,x') = Q(|x-x'|)$.

Nonlocal models can be divided into two groups, those treating internal nonlocality inside bulk junctions[14,15], and those dealing with nonlocal effects due to outer stray fields resulting from the geometry of the junction and its electrodes[16,17,18,19,20,21,22,23,24,25,26,27,28,29]. The latter group of theories takes into account the field configuration not only inside the junction,

but also around it, and incorporates the finite size of the sample and its shape-dependent magnetic properties. The shorter the junction is in x-direction (see Fig. 1), or the narrower it is in z- direction, the larger the effect of the geometrical nonlocality. Four typical geometries of long Josephson junctions are presented in Fig. 2. These are (a) edge-type, (b) ramp-type, (c) window and (d) overlap long junctions. In the ideal case of an infinitely long junction, the electrodynamic problem posed by (a)–(c) type junctions have been solved. In particular, theoretical models for the geometrical nonlocality have analyzed the following cases: 1) edge-type junctions between thick films $w \gtrsim \lambda_L$, neglecting internal nonlocal effects[21,29]; 2) edge-type junctions between thin films $w < \lambda_L$ (Pearl's limit)[18,28,30]; 3) edge-type and 4) ramp type junctions between films of arbitrary width, taking into account both the internal and external nonlocal problems[24,25]; 5) a variable thickness bridge above a ground plane[16,17] and 6) window junctions[20,26,27].

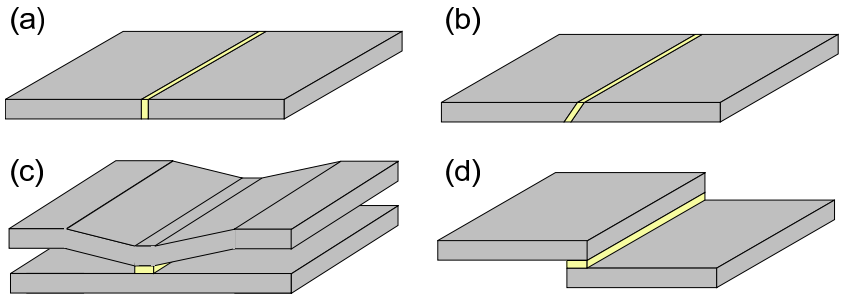

FIG. 2: Different geometries of long Josephson junctions formed between two superconducting films: (a) edge-type junction; (b) ramp-type junction; (c) window junction; (d) overlap junction.

In this paper, we study the effect of geometrical nonlocality by analyzing experiments on extremely narrow long Josephson junctions, down to a width w of 0.1 μm. The paper is organized as follows. In Sec. II we describe the geometries and preparation process of ultra-narrow low-T_c long Josephson junctions. In Sec. III we present experimental results obtained for Nb-AlO_x-Nb and Al-AlO_x-Al junctions. Theoretical models based on nonlocal electrodynamics, and their comparison with experiment, are presented in Sec. IV. Section V contains concluding remarks.

II. FABRICATION AND GEOMETRY OF ULTRA-NARROW LONG JOSEPHSON JUNCTIONS

The fabrication process of high quality long Josephson junctions in order to study the effects of nonlocal electrodynamics should satisfy the following three requirements: (i) ability to vary the junction width, from several micrometers down to several hundred nanometers, (ii) constant width along the junction length $L \gg \lambda_J$, which is typically several hundred micrometers, and (iii) an idle area of overlapping electrodes (window) that is as small as possible, so as to prevent it influencing wave propagation in the junction. We prepared samples using two different technologies based on aluminium and niobium. All samples were fabricated on a thermally oxidized Si substrates.

A. Al-AlO$_x$-Al junctions

The Al-AlO$_x$-Al junctions were prepared with the shadow evaporation technique. This method for the preparation of sub-μm Al-AlO$_x$-Al tunnel junctions is well known (see, e.g. Ref. 31). However, we cannot apply this method directly. A hanging bridge of electron resist (e.g. PMMA) or another material is usually used for shadowing during the evaporation of Al. As the length of the bridge becomes longer the bridge starts to sag. Thus, for long junctions (several hundred micrometers) the bridge cannot be well fixed. Therefore, in our preparation method, we use a *"shadowing window"*. Schematically the fabrication steps are shown in Fig. 3.

The first step was the formation of Au electrodes, used for spatially-uniform bias current injection and voltage measurement leads (Fig. 3 a). These electrodes were formed with the help of electron-beam lithography, thermal evaporation and the lift-off technique. The Cr layer under the Au layer improves Au adhesion to the substrate. The thicknesses of Cr and Au layers were 10 nm and 60 nm, respectively. The electrodes for current injection and voltage measurement across the junction have different geometries. One sees in Fig. 4 that the bias current leads have a length almost equal to that of the Josephson junction. The potential leads are much smaller, and are connected to the junction only at the edges of the Al electrodes. This geometry provides homogeneous current injection into long Josephson junctions and allows four point measurements of junction characteristics.

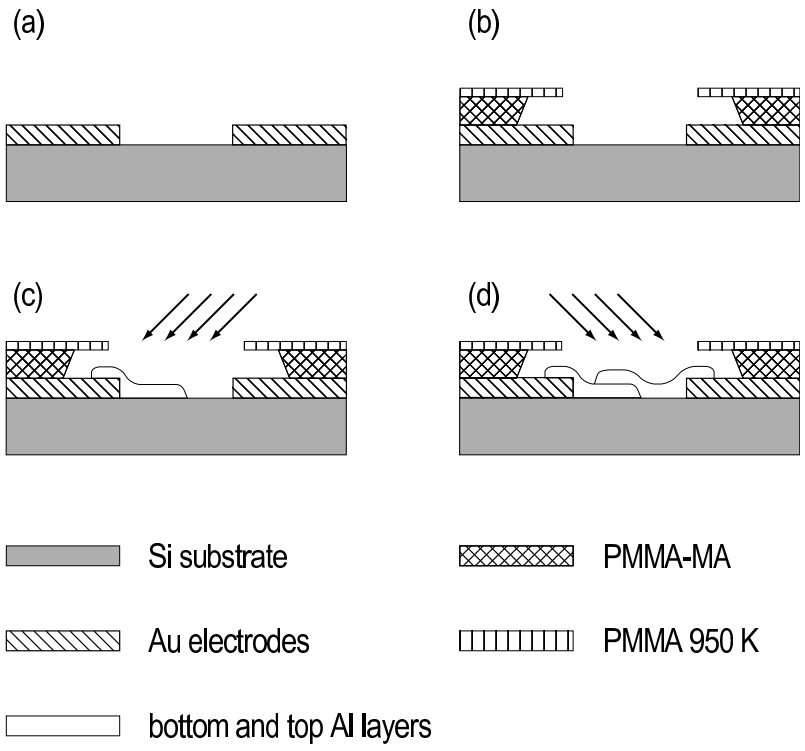

FIG. 3: Schematic diagram of the fabrication procedure for Al junctions. (a) Deposition of Au electrodes; (b) formation of a window in the PMMA resist for shadow evaporation; (c,d) deposition of top and bottom Al electrodes.

To form long Josephson junction by shadow evaporation, we used double layer resist PMMA-MA/PMMA 950 K, which was spanned onto the substrate with prepared electrodes. Then, using electron-beam lithography, we opened a window between the Au electrodes, as shown in Fig. 3 b. In the next step, we evaporated Al onto a tilted substrate (see Fig. 3 c). The thickness of this bottom Al layer was about 50 nm. Immediately after Al evaporation O_2 was injected into the vacuum chamber. The pressure of O_2 was kept at 10^{-3} mBar for 6 minutes. Then, a 200 nm thick top layer of Al was evaporated onto the tilted substrate (Fig. 3 d). The overlap of the bottom and top Al electrodes defines the junction area. A scanning electron micrograph of the resulting Josephson junction and electrodes is shown in Fig. 4.

Schematically, the cross section of the fabricated Josephson junction is shown in Fig. 5 a. Note that the total junction width is composed of two sections, one, of width w', parallel to the film surface plane and the other, of width w'', which is tilted. The total width is therefore $w = w' + w''$. Typically the relation $w'' \ll w'$ is well fulfilled. However, in the

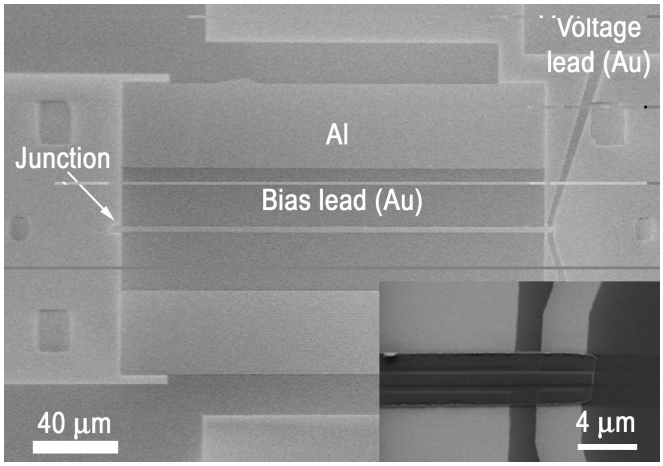

FIG. 4: SEM picture of Al-AlO_x-Al junction. The inset shows an enlarged view of the connection of current and potential electrodes to the junction.

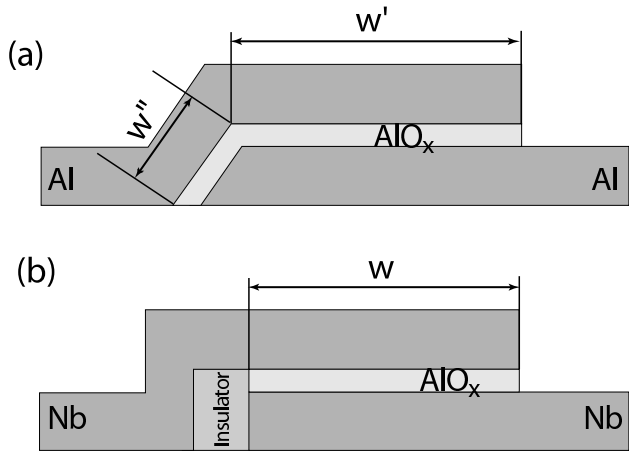

FIG. 5: Schematic cross sections of experimentally studied Al-AlO_x-Al (a) and Nb-AlO_x-Nb (b) junctions.

case of the most narrow junctions, the contribution of w'' to the junction width becomes significant. We estimate $w'' \simeq 60$ nm.

B. Nb-AlO_x-Nb junctions

There are several different approaches for the preparation of Josephson junctions using Nb-AlO_x-Nb trilayer technology. They differ mainly in patterning and insulation of the junction. Junctions with dimensions less than 1 μm usually have a window geometry (see Fig. 2 c), and are produced by reactive ion etching and vapor deposition of a dielectric layer.

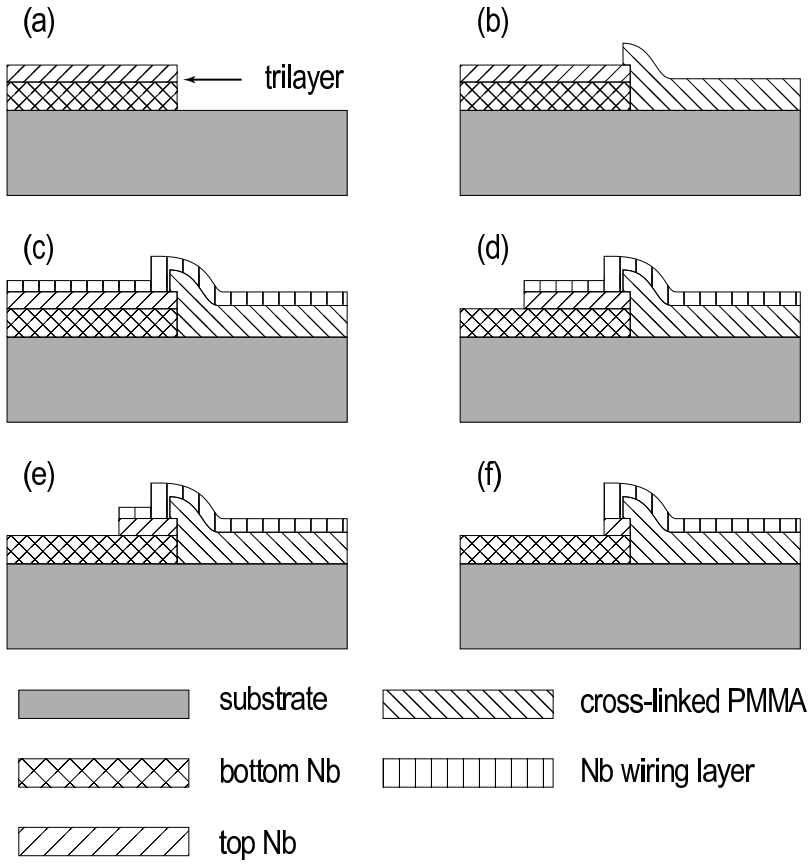

FIG. 6: Schematic diagram of the fabrication procedure for Nb junctions. (a) Formation of the trilayer; (b) insulation of the trilayer edge; (c) deposition of Nb wiring; (d) removal of Nb wiring and top Nb from all areas except that of the junction, (e,f) narrowing of the junction using electron beam lithography and reactive ion etching (repeated several times).

Using this approach, one could prepare sub μm junctions, however they would not satisfy the requirement of small idle region between the superconducting electrodes around the junction. In our group, we developed an alternative method, which allows junctions on the very edge of the Nb-AlO_x-Nb trilayer[10]. Schematically, this process is shown in Fig. 6. The junction cross section prepared in this way is shown in Fig. 5 b.

In the first step, the Nb-AlO_x-Nb trilayer region is defined by lithography and reactive ion etching (Fig. 6 a). The next step is the fine definition of one of the edges of the structure using electron beam lithography and etching. This particular edge was insulated by cross-linked PMMA (see Fig. 6 b). The details of the cross-linking procedure and the self-alignment of cross-linked PMMA along the trilayer edge can be found in Ref. 10. In the next step, the Nb wiring layer was deposited as shown in Fig. 6 c. Electron-beam lithography and reactive

TABLE I: Parameters of the measured junctions.

junction material	λ_L, nm	J_c, A/cm^2	λ_J, μm	$\bar{c}$, m/s,	$V_{\rm gap}$, mV
Al ($T = 0.3$ K)	15	270	56	$8 \cdot 10^6$	0.35
Al ($T = 0.9$ K)	17	160	68	–	0.29
Nb ($T = 4.2$ K)	90	210	25	$7 \cdot 10^6$	2.7

ion etching were used to define the junction area (see Fig. 6 d). After performing a full set of measurements on the junction, the width of the junction was iteratively decreased using electron beam lithography and reactive ion etching, as shown in Fig. 6 e and f.

III. EXPERIMENT

In this section, we present the data acquired for Al-AlO_x-Al and Nb-AlO_x-Nb ultra-narrow long Josephson junctions. A magnetic field H of up to 40 Oe was applied in the plane of the junction, perpendicular to its long dimension. The magnetic field of the Earth was screened out with a cryoperm shield. The experimentally determined parameters of the junctions are summarized in Table I. The London penetration depths for Al and Nb were found from period ΔH of $I_c(H)$ at high fields for widest junctions, as $\lambda_L = \Phi_0/(2L\Delta H)$. The Josephson penetration depth was found from the critical current density using Eq. (1). The Swihart velocity was found by fitting Fiske step voltages to the theoretical dependence (see Sec. IV C). The junction width was measured using a scanning electron microscope.

In the following, we describe two main effects observed in our ultra-narrow Josephson junctions, when the junction width w is decreased. These are 1) a reduction in the first critical field H_{c1}, and 2) an increase of the Fiske step voltage spacing ΔV_{FS}. According to standard (local) theory, the first critical field H_{c1} and the Fiske step voltage should not depend on the junction width[2].

The first critical field corresponds to the field when a single vortex enters the junction. In the local theory, the first critical field H_{c1} is inversely proportional to the Josephson penetration depth λ_J. In the following sections we present the experimental data for H_{c1} in terms of an effective length scale

$$\tilde{\lambda}_J = \frac{\Phi_0}{\pi H_{c1}(2\lambda_L + t)}. \tag{5}$$

Note that this equation is similar to the relation between λ_J and H_{c1} in the local theory.

Fiske steps arise when the Josephson oscillation frequency resonates with cavity modes of the junction. The voltages of these steps according to local theory are given by

$$V_n = \frac{\Phi_0}{2\pi}\frac{n\pi}{L}\bar{c} = \frac{\Phi_0}{2\pi}\frac{n\pi}{L}\omega_p\lambda_J, \tag{6}$$

where $\bar{c}$ is the Swihart velocity and n is the step number. Note that the Fiske step voltages V_n are also determined by the length scale λ_J, provided Josephson plasma frequency does not change.

A. Al-AlO$_x$-Al junctions

We measured a series of six 230 μm long Al-AlO$_x$-Al junctions. The width w of the junctions varied between 0.1 μm and 1 μm. The homogeneity of the junctions was verified by measuring the modulation pattern of the critical current I_c vs. field H at $T = 0.9$ K. In Fig. 7, $I_c(H)$ patterns of three samples of width $w = 0.11,\ 0.25$ and 0.82 μm are presented. We find the first critical field by linearly extrapolating the central peak in the critical current modulation pattern (see inset of Fig. 7). We observe that the first critical field H_{c1} decreases with decreasing the junction width w.

The experimentally determined effective length scale $\tilde{\lambda}_J$ is presented in Fig. 8 as black squares. This length scale depends strongly on the junction width. Theoretical curves are discussed below, in Sec. IV D.

Fiske steps of all junctions were measured by tracing the current-voltage characteristics during a continuous sweep of the external field H in the range from -40 Oe to $+40$ Oe. These measurements were performed at temperature $T = 0.3$ K, because at the higher temperature $T = 0.9$ K high damping suppresses the Fiske resonances. At $T = 0.3$ K the first critical field H_{c1} of the wide junctions ($w \simeq 0.6 - 0.8$ μm) was larger than the maximum field we could apply. In Fig. 9, the superimposed characteristics are plotted for the junction of width $w = 0.82$ μm.

We have observed that the positions of the Fiske steps strongly depend on the width of the junction. This dependence for the first step is shown in Fig. 10 and compared with the theory presented below in Sec. IV C.

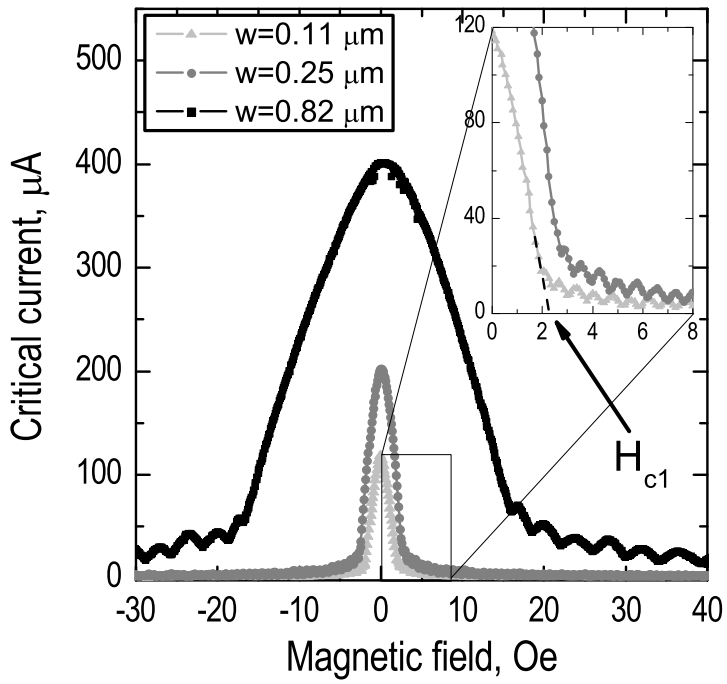

FIG. 7: Critical current modulation $I_c(H)$ in magnetic field for long Al-AlO_x-Al Josephson junctions at $T = 0.9$ K. The inset zooms in on the modulation patterns of the junctions of width $w = 0.11$ μm and $w = 0.25$ μm.

B. Nb-AlO_x-Nb junctions

Results of systematic measurements of ten long narrow Nb-AlO_x-Nb junctions were presented earlier in Ref. 10. We have now additionally measured three more junctions. Measurements were performed at temperature $T = 4.2$ K. In the present paper we analyze earlier data and our new results more extensively. The junction length is 200 μm and the width w ranges from 0.3 μm to 4.5 μm. The Josephson penetration depth was estimated from the critical current density using Eq. (1) to be about $\lambda_J \approx 25$ μm. The critical current vs. magnetic field patterns, reported in Ref. 10, and those of the new junctions show that all junctions are rather homogeneous. As in the case of the Al-AlO_x-Al junctions, a decrease in the first critical field H_{c1} (Fig. 11), and an increase of the Fiske step voltage spacing $\Delta V_{\rm FS}$ (Fig. 12), with decreasing width w of the junction were observed in the Nb-AlO_x-Nb junctions.

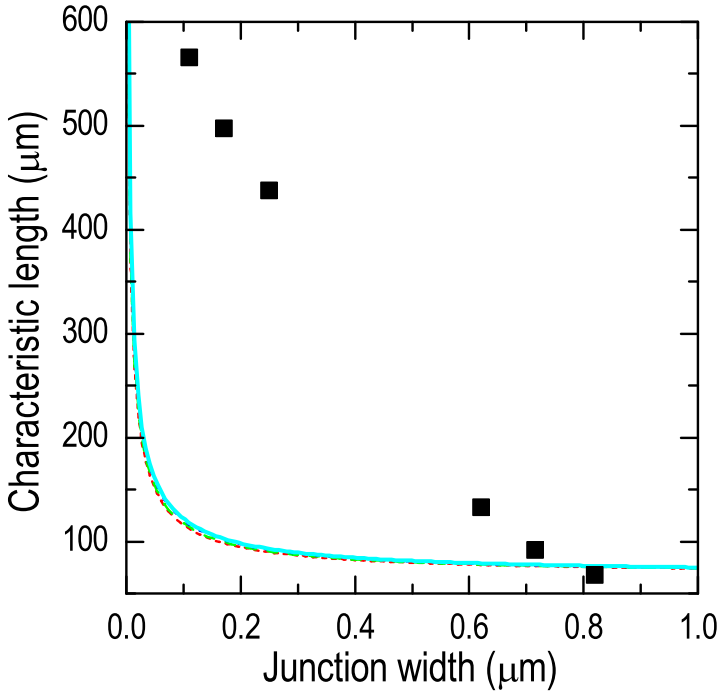

FIG. 8: Characteristic spatial scale of the Josephson phase in Al-AlO_x-Al junctions. Squares indicate the characteristic length scale $\tilde{\lambda}_J$, as extracted from the measured critical field H_{c1} at temperature $T = 0.9$ K, using to Eq. (5). Lines show theoretical estimations of the size $\tilde{\lambda}_J$ of a vortex, for details see Sec. IV D.

IV. COMPARISON WITH THEORY

In this section, we present a short review of the existing theoretical models for the nonlocal effects in edge-type Josephson junctions (Fig. 1). In particular, we are interested in the nonlocal kernels $Q(x, x')$ to be used in Eq. (4), and in the dispersion relation $\omega(k)$ of the junction, which determines the voltage position V_n of Fiske resonances. To compare with the experimental data, we include the frequency dependence of $\lambda_L(\omega)$ (material dispersion), and relate the critical magnetic field H_{c1} to the effective size of a vortex in the quasi-local limit.

A. Geometrical nonlocality

In a junction of finite length L the translational invariance along the junction is broken and, in general, the kernel $Q(x, x')$ depends not only on $x - x'$, but also on the sum $x + x'$

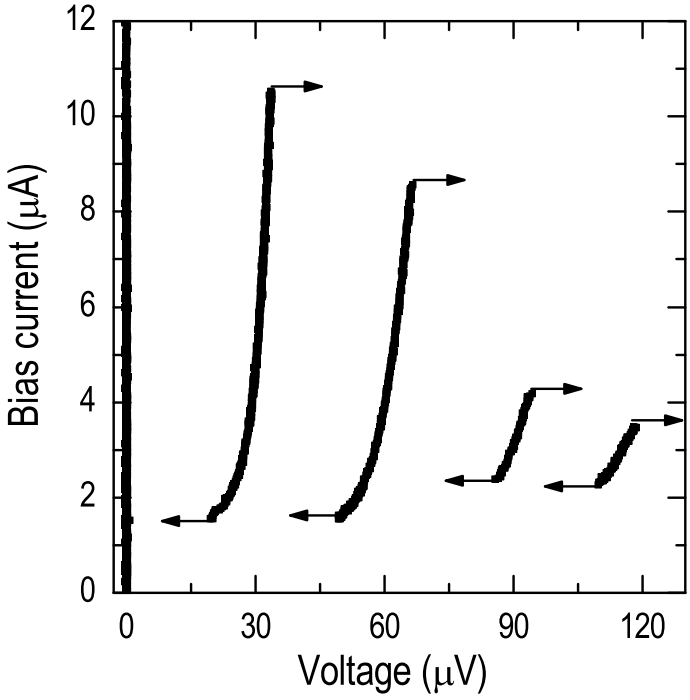

FIG. 9: Superimposed traces of Fiske resonances of the current-voltage characteristics of Al-AlO_x-Al long Josephson junctions at several different magnetic fields. The junction width is $w = 0.82$ μm and the temperature is $T = 0.3$ K.

and the length L. However, in a finite junction, deviations of the nonlocality kernel from the one of an infinitely long junction are expected, mainly in the edge region on the order of the magnetic screening length λ_L (or $\lambda_P = 2\lambda_L^2/w$ in thin films). These deviations can be neglected for the long junctions $L \gg \lambda_L$ ($L \gg \lambda_P$) considered in the following. This assumption is justified by the fairly good agreement obtained with the experimental data presented in figures 8, 10, 11, 12, 13 and 14.

We distinguish between nonlocal effects due to stray fields (and screening currents) inside and outside the junction electrodes. These two contributions are referred as internal and geometrical nonlocality, respectively.

(a) Let us first consider the theory for internal nonlocal effects in bulk junctions of width $w \gg \lambda_L$, see. Refs. 14,15. In this case the kernel in Eq. (4) is

$$Q(x) = (1/\pi\lambda_L)K_0(|x|/\lambda_L), \tag{7}$$

where K_0 is a modified Bessel function, having a logarithmic pole at $x \to 0$ and exponentially decaying at large distances[32]. Therefore, nonlocal effects become important here, when λ_L

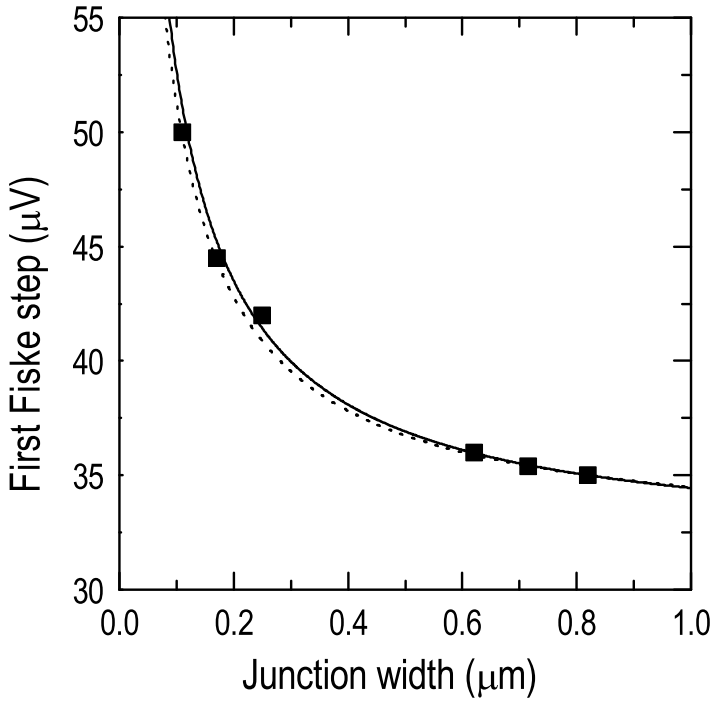

FIG. 10: The width dependence of the first Fiske step voltage V_1 for Al-AlO_x-Al junctions. Symbols correspond to experimental data obtained at $T = 0.3K$. The solid line corresponds to the theory of case[21] (c) and the dashed line to case[24] (d).

is large compared to the typical length scale l_φ, on which the phase varies , i.e. in the case of $\lambda_L \geq \lambda_J$. In the limit $\lambda_L \ll \lambda_J$ the local sine-Gordon equation is recovered.

Usually λ_J is much larger than λ_L, because the critical current density j_c in the junction is much smaller than the critical (depairing) current density $j_d = 2\Phi_0/(3\sqrt{3}\pi^2\mu_0\lambda_L^2\xi)$ in the bulk superconductor (ξ is the coherence length). Exceptions are, for example, junctions in high-temperature superconductors created by planar defects such as twins, stacking faults, low-angle grain boundaries, etc[33]. These structural defects often form Josephson junctions with high j_c and therefore small λ_J. In terms of the critical current density across the junction, the condition $\lambda_J < \lambda_L$ is fulfilled if $j_d/\kappa < j_c < j_d$, where $\kappa = \lambda_L/\xi$ is the Ginzburg-Landau parameter[14]. Note that for extreme type-II superconductors, $\kappa \gg 1$, the relation $\lambda_J < \lambda_L$ holds over a wide range of j_c.

Linearizing the wave equation (4) ($\sin\varphi \simeq \varphi$), one obtains the dispersion relation $\omega(k)$ for small-amplitude linear electromagnetic waves $\varphi(x,t) = \varphi_0 \exp(-\mathrm{i}\omega t + \mathrm{i}kx)$ (here $|\varphi_0| \ll 1$)

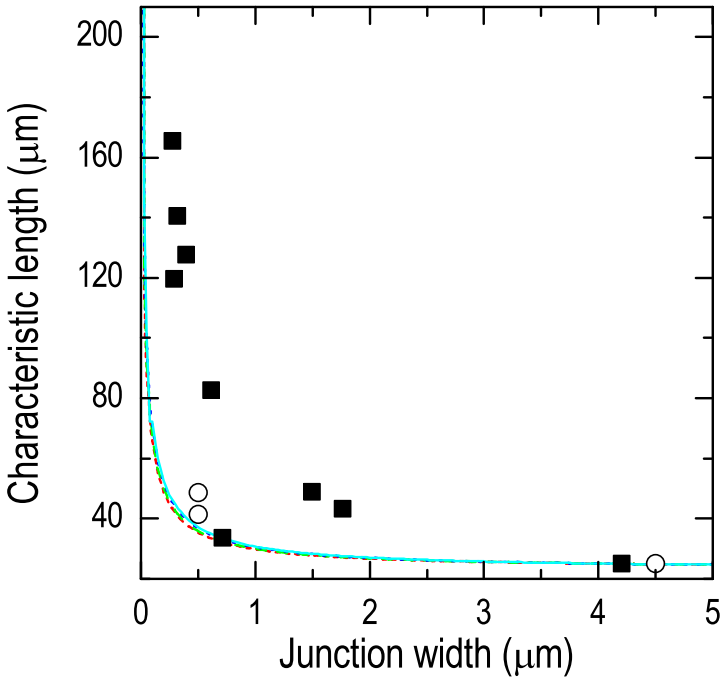

FIG. 11: Characteristic spatial scale of the Josephson phase in Nb-AlO_x-Nb junction at $T = 4.2$ K. The open circles denote the length scale $\tilde{\lambda}_J$ extracted from the experimental critical field H_{c1} according to Eq. (5) for new junctions. The solid symbols correspond to experimental data for H_{c1} of Ref. 10. Lines correspond to the theoretical estimations of the size $\tilde{\lambda}_J$ of a vortex (see Sec. IV D).

propagating along a Josephson junction. From the above kernel it follows that

$$\omega = \omega_p \left(1 + \frac{k^2 \lambda_J^2}{\sqrt{1 + k^2 \lambda_L^2}} \right)^{\frac{1}{2}}. \tag{8}$$

(b) The geometrical nonlocality of an edge-type junction formed between two thin superconducting films $w < \lambda_L$ (Fig. 2(a)) has been extensively studied[18,22,28]. In this case, the stray fields outside the junction area account for the entire electromagnetic energy of the junction. The typical length scale upon which magnetic fields vary, is not the London penetration depth λ_L, but the Pearl penetration depth[30] $\lambda_P = 2\lambda_L^2/w \gg \lambda_L$. The nonlocality kernel is then given by[28]

$$\begin{aligned} Q(x) &= \frac{4\lambda_L}{w} \int \frac{dkdq}{(2\pi)^2} \frac{\exp(\mathrm{i}kx)}{\sqrt{k^2+q^2}[1+\lambda_P^2 q^2]} \\ &= \frac{1}{2\lambda_L} \left(\mathrm{H}_0 \left(\frac{|x|}{\lambda_P} \right) - Y_0 \left(\frac{|x|}{\lambda_P} \right) \right), \end{aligned} \tag{9}$$

where H_0 and Y_0 are the Struve and Bessel function of the second kind[32]. As in the previous case, this kernel has a logarithmic pole at $x \to 0$, however at large distances it decays as

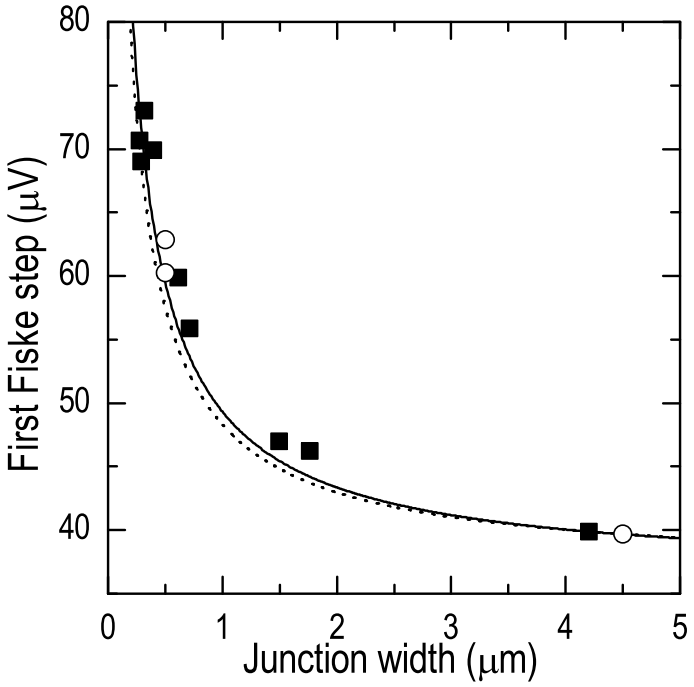

FIG. 12: The width dependence of the maximum of the first Fiske step voltage V_1 for Nb-AlO_x-Nb junctions. The open symbol correspond to new experimental data and the data for solid symbols are taken from Ref. 10. The solid line is calculated using the theory of Ref. 21 and the dashed line corresponds to the theory of Ref. 24.

$\sim 1/x$. When the phase variation length l_φ is large compared to the magnetic screening length, $\lambda_P \ll l_\varphi$, the characteristic vortex size is given by $\tilde{\lambda}_J = l_\varphi = \lambda_J(\lambda_L/w)^{1/2} \gg \lambda_J$. The limit of $\lambda_P \ll l_\varphi$ is then equivalent to $\lambda_L \ll \lambda_J(w/\lambda_L)^{1/2}$. In the opposite limit of $l_\varphi \ll \lambda_P$ or $\lambda_L \gg \lambda_J(w/\lambda_L)^{1/2}$ the length scales for the tails ($\tilde{\lambda}_J$) and the core (λ_J^2/λ_L) of a Josephson vortex are different[28].

(c) Ivanchenko's theory[21] applies to edge-type junctions of width larger than the London penetration depth, $w \gtrsim \lambda_L$. This model assumes that stray fields outside the film affect only the surface, and that the interior of the junction is described by the local theory. In this case the integral kernel has the form[21]:

$$\begin{aligned} Q(x) &= \delta(x) + \frac{4\lambda_L}{w}\int \frac{dkdq}{(2\pi)^2}\frac{\exp(\mathrm{i}kx)}{\sqrt{k^2+q^2}[1+\lambda_L^2 q^2]} = \\ &= \delta(x) + \frac{1}{w}\left(\mathbf{H}_0\left(\frac{|x|}{\lambda_L}\right) - Y_0\left(\frac{|x|}{\lambda_L}\right)\right) \end{aligned} \tag{10}$$

Note that the second term is identical to the kernel of Eq. (9), corresponding to the case of a

thin film junction, but the Pearl penetration depth λ_P is replaced by the London penetration depth λ_L. As in the previous case, when l_φ is large compared to the typical length scale of the kernel, $\lambda_L \ll l_\varphi$, the vortex size is given by $\tilde{\lambda}_J = l_\varphi = \lambda_J(1+\lambda_L/w)^{1/2}$.

In the limit of $l_\varphi \gg \lambda_L$ for cases (b) and (c), Eq. (4) does not transform exactly into the local sine-Gordon equation with effective length scale $\tilde{\lambda}_J$, because $Q(x)$ does not correspond to $\delta(x)$ for $\lambda_{P/L} \to 0$. Nevertheless, the locality of the kernel suggests that in this limit an effective local sine-Gordon equation with renormalized Josephson penetration depth $\tilde{\lambda}_J$ should be qualitatively correct. Then one could use the expressions for H_{c1} and $\bar{c} = \omega_{\rm p}\lambda_J$ from local theory, if λ_J is replaced by a new length $\tilde{\lambda}_J$, see below.

In the absence of dissipation and bias current, using the kernel (10) we obtain the dispersion relation for this case as

$$\omega(k) = \omega_p \sqrt{1 + k^2\lambda_J^2 + \frac{4k^2\lambda_J^2\Lambda}{\pi w\sqrt{k^2\Lambda^2 - 4}} \arccos\left(\frac{2}{|k|\Lambda}\right)} \tag{11}$$

for $k\Lambda \geq 2$ and

$$\omega(k) = \omega_p \sqrt{1 + k^2\lambda_J^2 + \frac{4k^2\lambda_J^2\Lambda}{\pi w\sqrt{4 - k^2\Lambda^2}} \,\mathrm{arccosh}\left(\frac{2}{|\mathrm{k}|\Lambda}\right)} \tag{12}$$

for $k\Lambda < 2$.

(d) The theory developed by Lomtev and Kuzovlev[24] is the most general as it contains the special cases (a)-(c) discussed above. It assumes that the phase $\varphi(x)$ does not vary over the width w. The kernel is

$$Q(x) = \frac{1}{\pi\lambda_L} K_0\left(\frac{|x|}{\lambda_L}\right) + \frac{2}{\pi w\lambda_L^3} \int_0^\infty \frac{dq J_0(qx)}{\kappa^3(\kappa + q\coth(\kappa w/2))}, \tag{13}$$

where $\kappa = (q^2 + 1/\lambda_L^2)^{1/2}$, J_0 is the Bessel function of the first kind. In this case the dispersion relation in the absence of perturbation terms in Eq. (4) is[24]

$$\omega(k) = \omega_p \sqrt{1 + \frac{k^2\lambda_J^2}{\sqrt{1 + k^2\lambda_L^2}} + \frac{k^2\lambda_J^2}{\pi\lambda_L} F(k)} \quad , \tag{14}$$

where

$$F(k) = \frac{2}{w\lambda_L^2} \int_k^\infty dq \frac{1}{\kappa^3} \frac{1}{\kappa + k\coth(\kappa w/2)} \frac{1}{(q^2 - k^2)^{1/2}} \quad . \tag{15}$$

This theory has also been generalized to describe ramp-type junctions[25] (Fig. 2(b)).

Let us quote typical parameters for our low-T_c long Josephson junctions. For the Nb-AlO_x-Nb junctions considered in this paper $\lambda_J \simeq 25$ μm, and $\lambda_L \simeq 90$ nm at $T = 4.2$ K, and for Al-AlO_x-Al junctions $\lambda_J \simeq 56$ μm and $\lambda_L \simeq 15$ nm at T=0.3 K, and $\lambda_J \simeq 68$ μm and $\lambda_L \simeq 17$ nm at T=0.9 K. For these parameters, the condition $\lambda_L \ll \lambda_J$ is fulfilled in all cases, i.e. the internal nonlocal effects as discussed in case (a) are negligibly small. For Al-AlO_x-Al junctions $w \approx 0.1 - 0.8$ μm, and for Nb-AlO_x-Nb junctions $w \approx 0.3 - 4.2$ μm, which is significantly larger than λ_L. It is reasonable to expect that our junctions can be approximately described by the theory presented in Ref. 21. In the following analysis, we compare our experimental data with Ivanchenko's theory[21], case (c) and with the more general theory of Lomtev and Kuzovlev[24], case (d).

B. Material dispersion

We will see in Sec. IV C, that for small frequencies the nonlocal dispersion relation predicts a strong decrease of the spacing between the Fiske steps $\Delta V_{FS\ n} = V_n - V_{n-1}$ with increasing n (cf. Eqs. (11), (12), (14) and (21)). For large wave numbers, this effect is of the same order of magnitude as the reduction of the spacing between Fiske steps due to material dispersion[12]. Material dispersion arises from the frequency dependence of the complex conductivity and surface impedance of the superconducting electrodes[11,13]. It leads to a frequency dependence of λ_L which becomes significant at frequencies on the order of the superconducting energy gap frequency $f_{\rm gap} = \Delta/h$ (Δ is the superconducting energy gap). The gap frequency of the Nb-AlO_x-Nb junctions is $f_{\rm gap} \simeq 650$ GHz (at 4.2 K) and that of Al-AlO_x-Al is $f_{\rm gap} \simeq 85$ GHz (at 0.3 K). The frequency dependence of λ_L can be written as[11,12]

$$\left(\frac{\lambda_L(0)}{\lambda_L(\omega)}\right)^2 = \sqrt{\pi\Delta} \int\limits_{\Delta-\hbar\omega}^{\Delta} dx\,[1 - 2f\,(x+\hbar\omega)]\,\frac{x^2+\Delta^2+x\hbar\omega}{\sqrt{\Delta^2-x^2}\sqrt{(x+\hbar\omega)^2-\Delta^2}}, \qquad (16)$$

where $f(x) = 1/(1+e^{x/k_BT})$ is the Fermi-Dirac distribution function, k_B is Boltzmann's constant.

C. Fiske steps

Let us consider a long junction of finite length L in the direction of wave propagation. Because of reflection at the edges, it behaves like a resonant transmission line and supports cavity modes of the electromagnetic field. The theory of such resonances (Fiske resonances) in the local case was developed by Kulik[34,35]. The nonlocal theory for semi-infinite, and finite Josephson junctions[19,36] suggest that for case (c) of Ivanchenko[21], in the presence of an external magnetic field H_e, we can use the boundary condition

$$\varphi_x(0) = \varphi_x(L) = \frac{2\pi\Lambda}{\Phi_0} H_e. \tag{17}$$

Then, the Josephson phase is written as

$$\varphi = \omega t - kx + \varphi_1(x,t) \tag{18}$$

where $\omega = 2\pi V/\Phi_0$ and $k = 4\pi\lambda_L H_e/\Phi_0$. As a first approximation, we consider $\varphi_1(x,t)$ as a small perturbation. By inserting this into Eq. (4) we obtain

$$\lambda_J^2 \frac{\partial}{\partial x} \int dx' Q(x-x')\varphi_{1,x'}(x') - \omega_p^{-2}\varphi_{1,tt} - \omega_p^{-1}\alpha\varphi_{1,t} = \sin(\omega t - kx), \tag{19}$$

where we neglect $\varphi_1(x,t)$ in the sine term, and use the assumption concerning the nonlocality kernel made at the beginning of Sec. IV A. Furthermore, $\varphi_1(x,t)$ can be expanded in terms of the normal modes of the junction

$$\varphi_1(x,t) = \mathrm{Im}\left\{ \sum_{n=0}^{\infty} g_n e^{\mathrm{i}\omega_n t} \cos k_n x \right\}, \tag{20}$$

where g_n are complex numbers, $k_n = n\pi/L$. This choice for the x dependence implies the boundary conditions $\varphi_{1,x}(0) = \varphi_{1,x}(L) = 0$, which is consistent with (17). The frequency ω_n is determined from the dispersion relation of Eq. (19), namely $\sqrt{\omega^2(k) - \omega_p^2}$, $\omega(k)$ is determined in Sec. IV A. By inserting the expression (20) for φ_1 into Eq. (19), and solving the set of the equations for g_n, we obtain the following expression for the position of the Fiske resonances

$$V_n = \frac{\hbar}{2e}\sqrt{\omega^2(k_n) - \omega_p^2}. \tag{21}$$

In the local case ($Q(x) = \delta(x)$, $\omega^2(k) = \omega_p^2 + \bar{c}k^2$) we obtain Eq. (6).

Using Eqs. (11), (12), (14)-(16) and (21), in Fig. 10 we plot the dependence of the first Fiske step voltage V_1 on the junction width w for Al-AlO$_x$-Al junctions, and in Fig. 12 that

for Nb-AlO_x-Nb junctions. The only fitting parameter for all curves is the Swihart velocity. For the Al-AlO_x-Al junctions we found $\bar{c} \simeq 8 \times 10^6$ m/s and for Nb-AlO_x-Nb junctions $\bar{c} \simeq 7 \times 10^6$ m/s. The Swihart velocity found using the theory of case[21] (c) and that of case[24] (d) differ by about 1%. This small difference indicates that internal nonlocal effects, taken into account in case (d), are negligibly small in our junctions.

In Figs. 13 and 14 we compare the measured (symbols) voltage positions V_n of the Fiske steps to theoretical curves calculated from Eqs. (11), (12), (14)-(16) and (21), where both nonlocality and material dispersion have been taken into account. Solid lines correspond to the theory of case[21] (c), and dashed lines to the theory of case[24] (d). The data for Al junctions is presented in Fig. 13, and for Nb junctions presented in Fig. 14. The difference between the curves according to the two theories decreases with increasing the width of the junctions. For the Nb-AlO_x-Nb junction of width 4.2 μm the difference cannot be distinguished.

Thus, our experimental data for Fiske steps in both Al-AlO_x-Al and Nb-AlO_x-Nb junctions are in good agreement with theory[21,24].

D. Critical magnetic fields and vortex size

For a junction placed in an external magnetic field the integro-differential equation (4) contains an additional Meissner current $j_m(x, y, z)$, which is also induced in the absence of the junction and depends on the size and the shape of the electrodes (demagnetization effects). If the dynamics of the phase inside a small surface region of size $\sim \lambda_L \ll L, \tilde{\lambda}_J$ is disregarded, the geometry dependent current j_m can formally be taken into account by supplying the nonlocal wave equation for the case of infinite length with appropriate (nonlocal) boundary conditions. Physically, these boundary conditions reflect edge capacitances and inductances, and take into account the stray field in the xy-plane for $-w/2 \leq z \leq w/2$, in addition to the stray fields above and below the superconducting leads, which are contained in the nonlocal kernel $Q(x)$. These boundary conditions depend on the global geometry of the sample and the magnetic screening length in addition to the kernel Q. The magnetic penetration field H_{c1} is therefore more difficult to interpret theoretically than the Fiske steps, which follow from the kernel Q alone.

Although in general the solution is difficult to find, in the physically relevant case (c) for

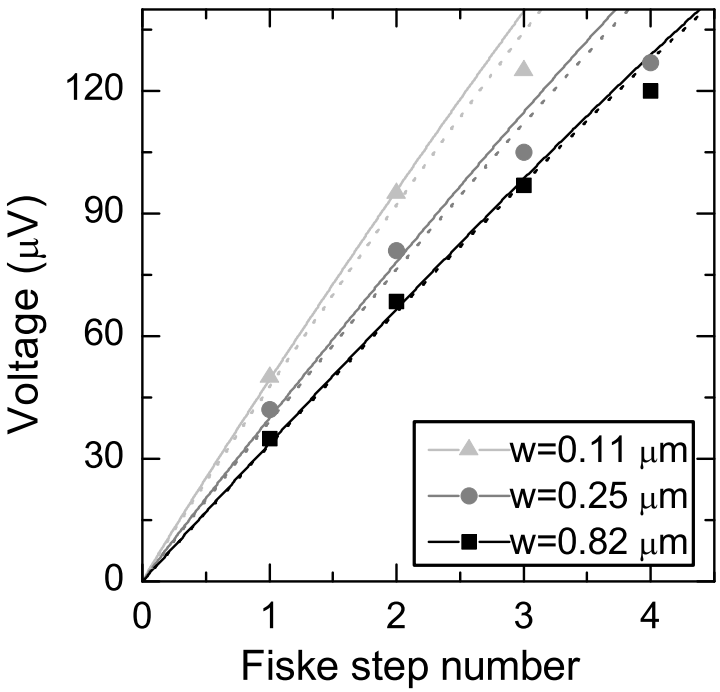

FIG. 13: Comparison of experimentally obtained Fiske step voltages for Al-AlO_x-Al junctions of different widths (symbols) with the dispersion curve calculated from nonlocal theories taking into account material dispersion (lines). Triangles correspond to the junction of width $w = 0.11\,\mu$m, circles to $w = 0.25\,\mu$m and rectangles to $w = 0.82\,\mu$m. The solid line corresponds to the theory of case[21] (c) and the dashed line to case[24] (d).

$\lambda_L \ll l_\varphi$, where the Eq. (4) transforms into the local sine-Gordon equation with an effective length scale $\tilde{\lambda}_J$, the expressions for H_{c1} and $\bar{c} = \omega_p \lambda_J$ from the local theory can be used. In doing so the correct magnetic screening length, e.g. λ_L for $w \gtrsim \lambda_L$, and the effective vortex size $\tilde{\lambda}_J = \lambda_J(1 + \lambda_L/w)^{1/2}$ from the effective local theory has to be used. Assuming that bulk material properties like j_c do not depend on the junction width w, it is possible to obtain the scaling relation[10]

$$\bar{c}(w) \sim \frac{1}{H_{c1}^{1/3}(w)} \tag{22}$$

between these quantities, when the width w is changed, which is well satisfied experimentally[10]. Even if the effective local theory provides a good approximation for the static case, it might nevertheless fail to describe in the dynamic case some significant properties of the junction, such as the possibility of Cherenkov radiation above a critical velocity (similarly for the internal nonlocality[23]).

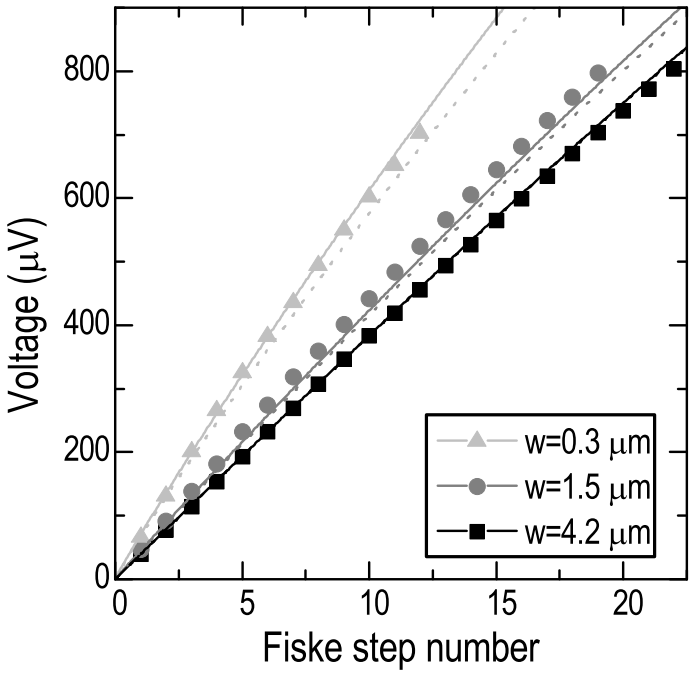

FIG. 14: Comparison of experimentally obtained Fiske step voltages for Nb-AlO_x-Nb junctions of different widths (symbols) with the dispersion curve calculated from nonlocal theories taking into account material dispersion (lines). Triangles correspond to the junction of width $w = 0.3\,\mu$m, circles to $w = 1.5\,\mu$m and rectangles to $w = 4.2\,\mu$m. The solid line corresponds to the theory of case[21] (c) and the dashed line to case[24] (d).

We will now verify the correct choice of the length scale $\tilde{\lambda}_J$ of a Josephson vortex using a variational approach. As the variation parameter we take the vortex size $\tilde{\lambda}_J$, and minimize the Lagrange function of the unperturbed ($\alpha = \gamma = 0$) nonlocal sine-Gordon equation (4)

$$\frac{\mathcal{L}}{E_J w} = \int dx \left(\frac{1}{2}\frac{1}{\omega_p^2}\varphi_t^2 - (1-\cos\varphi) \right) - \frac{1}{2}\lambda_J^2 \int dxdy\ \varphi_x(x)\varphi_y(y)Q(x-y) \qquad (23)$$

$$(24)$$

As trial functions we took the two limiting solutions of Eq. (4). For $w \to \infty$, the vortex solution of Eq. (4) is an exponential kink[37]

$$\varphi(x,\tilde{\lambda}_J) = 4\arctan\left(\exp\frac{x}{\tilde{\lambda}_J}\right), \qquad (25)$$

The other limit is $w \to 0$, for which the one vortex solution decays algebraically[28]:

$$\varphi(x,\tilde{\lambda}_J) = 2\arctan\frac{x}{\tilde{\lambda}_J} + \pi. \qquad (26)$$

Here $\tilde{\lambda}_J$ is considered as a free variational parameter corresponding to the characteristic size of the vortex. The results for Al-AlO_x-Al junctions calculated from the first critical field H_{c1} at $T = 0.9$ K are presented in Fig. 8 by symbols. The lines correspond to variational results for the theories of Refs. 21 and 24 with the above two ansatzes. Each curve was fitted to the experimental data for junction widths in the range $0.7 - 0.8$ μm. The prefactors for different theories differ by 3 %. Figure 11 presents the characteristic vortex size $\tilde{\lambda}_J$ as a function of junction width for Nb-AlO_x-Nb junctions, for $T = 4.2$ K and $\lambda_L = 90$ nm. In this figure the curves are fitted to the experimental data point at width $w = 4.2\mu$m. One notes that in both cases all four curves overlap with each other.

The agreement between experimental data (symbols) and theoretical estimations (lines) in Figs. 11, 8 is rather poor. We suppose this is due to the fact that none of the theories properly consider the boundary conditions at the edges of a junction. Deriving appropriate boundary conditions for realistic junction geometries in the nonlocal case remains an unsolved problem, which requires further work.

E. Vortex mass

Finally, we would like to discuss the effect of nonlocal electrodynamics on the dynamical mass and quantum behaviour of Josephson vortices. We note that the first experiment with a vortex in the quantum regime was presented in Ref. 5. The (nonrelativistic) mass m_F of a Josephson vortex, which appears in the equation of motion

$$m_F \ddot{q} + \frac{\partial \mathcal{H}_{\rm ext}}{\partial q} = 0 \tag{27}$$

for the vortex center of mass coordinate q in an external potential $\mathcal{H}_{\rm ext}$, is obtained by expanding the Lagrange function

$$\mathcal{L} \approx \frac{1}{2} m_F v^2 - H_{\rm ext} + {\rm const} \tag{28}$$

of Eq. (23) in terms of $v \ll \bar{c}$. The spacing $\hbar\omega_0$ between the energy levels (and, thus, zero point fluctuations) is then given by

$$\omega_0^2 = \frac{1}{2m_F} \frac{\partial^2 H_{\rm ext}}{\partial q^2}. \tag{29}$$

The condition $\hbar\omega_0 > k_B T$ is required for dominantly quantum behaviour of the fluxon. In the limit $m_F \to 0$, the spectrum becomes discrete, provided that the energy scale of the potential is fixed.

The external potential $\mathcal{H}_{\rm ext}$ for a vortex in a Josephson junctions can be, for example, induced by an external magnetic field or by presence of a micro-short (micro-resistor). In the first case, the external magnetic field creates a screening current flowing through the junction. Provided that the nonlocality of the magnetic screening at the edges can be neglected or, equivalently, Eq. (17) for the boundary condition is justified, the current spreads homogenously over the width of the junction. Hence, the external potential $\mathcal{H}_{\rm ext}$ is proportional to the junction width[38]. In the second case, the inhomogeneity leads to a local change in the Josephson energy. If the magnitude of the inhomogeneity is constant across the junction, the total change in the Josephson energy is proportional to w. As we see, in both situations the external potential $\mathcal{H}_{\rm ext}$ scales with w, hence, for characterizing the degree of quantum behavior, the use of the *specific* mass $\tilde{m}_F = m_F/w$ for a vortex is more appropriate than using the mass m_F.

For local theory ($\lambda_J \gg w \gg \lambda_L$), the mass of a vortex of form (25) is given by

$$m_F = \frac{8 E_J w}{\omega_p^2 \lambda_J}, \tag{30}$$

which vanishes in the limit $w \to 0$, whereas the specific mass $\tilde{m}_F = m_F/w$ is constant.

Similarly, in the nonlocal case we make use of the ansatz $\phi(x,t,v) = \tilde{\phi}(\tilde{x}, v)$, where $\tilde{x} = (x - vt)/\tilde{\lambda}_J(v)$ and $\tilde{\lambda}_J(v)$ is the characteristic length scale of the vortex, which in general depends on the velocity (cf. the Lorentz-factor $1/\sqrt{1-(v/\bar{c})^2}$ in the local case), and which can be determined from the variational ansatz. As the Lorentz invariance is broken in the nonlocal case, we do not know a priori the functional dependence of ϕ on v, and an additional explicit dependence on v is possible, if the shape of the vortex depends on v. From (23) we obtain

$$\frac{\mathcal{L}}{E_J w} = \frac{1}{2\omega_p^2}\frac{1}{\tilde{\lambda}_J} I_1 v^2 + \tilde{\lambda}_J I_2 + \frac{\lambda_J^2}{2}\, I_3\left(\tilde{\lambda}_J(v), \lambda_L, w\right), \tag{31}$$

where

$$I_1 \;=\; \int d\tilde{x}\;(\tilde{\varphi}'(\tilde{x}))^2; \tag{32}$$

$$I_2 \;=\; -\int d\tilde{x}\;(1-\cos\tilde{\varphi}); \tag{33}$$

$$I_3 \;=\; -\int d\tilde{x}\;d\tilde{y}\;\tilde{\varphi}'(\tilde{x})\tilde{\varphi}'(\tilde{y})Q(\tilde{\lambda}_J|\tilde{x}-\tilde{y}|). \tag{34}$$

The effective mass in the nonlocal case is obtained by expanding $\mathcal{L}(v)$ into second order. Neglecting the explicit dependence on v, and expanding

$$\tilde{\lambda}_J(v) = \tilde{\lambda}_{J0} + \frac{1}{2}\frac{d^2\tilde{\lambda}_J}{dv^2}v^2 = \tilde{\lambda}_{J0} + \frac{1}{2}\frac{v^2}{\tilde{c}^2}, \tag{35}$$

one obtains

$$m_f = \frac{E_J w}{\omega_p^2}\frac{I_1}{\tilde{\lambda}_{J0}} + \frac{E_J w}{2}\frac{d^2\tilde{\lambda}_J}{dv^2}\left(2I_2 + \lambda_J^2\frac{\partial I_3(\tilde{\lambda}_J=\tilde{\lambda}_{J0})}{\partial\tilde{\lambda}_J}\right). \tag{36}$$

Here we again apply the variational approach as we did to obtain the vortex size. Then the expression in brackets is the Lagrange equation for the variation parameter $\tilde{\lambda}_{J0}$, and is therefore equal to zero. Thus the effective mass for the trial function of the form (25) can explicitly be written as

$$m_f = \frac{8E_J w}{\omega_p^2\tilde{\lambda}_{J0}}. \tag{37}$$

Since $\tilde{\lambda}_J$ increases with w, both the effective mass m_f and the specific mass m_f/w (responsible for the energy scaling, if $\mathcal{H}_{\rm ext} \sim w$) decrease with decreasing the junction width. From Eq. (37) one notes that the inverse of the specific mass scales with the characteristic length $\tilde{\lambda}_{J0}$ (see Figs. 8 and 11).

Let us emphasize again that the possibility of a vortex behaving as a macroscopic quantum particle, when reducing the width w of the junction, not only depends on the scaling of the (kinetic) mass m_F, but more exactly the ratio of the kinetic energy to the external potential $\mathcal{H}_{\rm ext}$, which has to be determined for each specific experimental situation.

V. CONCLUSION

The current-voltage characteristics and critical current versus field patterns of narrow long Josephson junctions show a strong dependence on the junction width w. This cannot be explained using the conventional theory based on the local sine-Gordon model. Our experimental data are well described by the nonlocal theory originally developed by Ivanchenko[21],

and later extended by Lomtev and Kuzovlev[24]. According to these models, the electrodynamic and static properties of a junction depend on the junction width. Our experimental data for Fiske steps observed in both Al-AlO_x-Al and Nb-AlO_x-Nb long narrow junctions are in very good quantitative agreement with these theories. The dependence of the first critical field on the width of the junction allows qualitative estimates of the characteristic vortex size, which is influenced by nonlocal effects. A proper description of the static effects requires a better treatment of the boundary conditions at the edges of a junction.

We also calculate the specific mass of a vortex in the nonlocal case. According to local theory, the specific mass does not depend on the junction width w. By contrast, the nonlocal theory predicts that the specific mass of a vortex decreases with decreasing junction width.

VI. ACKNOWLEDGEMENTS

We would like to thank M. V. Fistul for useful discussions and A. Price for careful reading of this manuscript.

---

* Electronic address: abdumalikov@physik.uni-erlangen.de

[1] I. O. Kulik and I. K. Yanson, *The Josephson Effect in Superconducting Tunnel Structures* (Keter Press, Jerusalem, 1972).

[2] A. Barone and G. Paternó, *Physics and Applications of the Josephson Effect* (Willey, New York, 1982).

[3] K. K. Likharev, *Dynamics of Josephson Junctions and Circuits* (Gordon and Breach, New York, 1986).

[4] A. V. Ustinov, Physica D **123**, 315 (1998).

[5] A.Wallraff, A.Lukashenko, J.Lisenfeld, A.Kemp, M.V.Fistul, Y. Koval, and A. Ustinov, Nature **425**, 155 (2003).

[6] M. V. Fistul, A. Wallraff, Y. Koval, A. Lukashenko, B. A. Malomed, and A. V. Ustinov, Phys. Rev. Lett. **91**, 257004 (2003).

[7] Z. Hermon, A. Stern, and E. Ben-Jacob, Phys. Rev. B **49**, 9757 (1994).

[8] T. Kato and M. Imada, J. Phys. Soc. Jpn. **65**, 2963 (1996).

[9] A. Shnirman, E. Ben-Jacob, and B. Malomed, Phys. Rev. B **56**, 14677 (1997).

[10] Y. Koval, A. Wallraff, M. Fistul, N. Thyssen, H. Kohlstedt, and A. V. Ustinov, IEEE Trans. Appl. Supercond. **9**, 3957 (1999).

[11] D. C. Mattis and J. Bardeen, Phys. Rev. **111**, 412 (1958).

[12] G. S. Lee and A. T. Brafknecht, IEEE Trans. Appl. Superconduct. **2**, 67 (1992).

[13] M. Tinkham, *Introduction to Superconductivity* (McGraw-Hill, New York, 1996), 2nd ed.

[14] A. Gurevich, Phys. Rev. B **46**, R3187 (1992).

[15] Y. M. Aliev, V. P. Silin, and S. A. Uryupin, Superconductivity **5**, 1992 (1992).

[16] G. M. Lapir, K. K. Likharev, L. A. Maslova, and V. K. Semenov, Fiz. Niz. Temp. (Sov. J. Low Temp. Phys.) **1**, 1235 (1975).

[17] M. Y. Kupriyanov, K. K. Likharev, and V. K. Semenov, Fiz. Niz. Temp. (Sov. J. Low Temp. Phys.) **2**, 706 (1976).

[18] Y. M. Ivanchenko and T. K. Soboleva, Phys. Lett. A **147**, 65 (1990).

[19] V. G. Kogan, Phys. Rev. B **49**, 15874 (1994).

[20] N. Thyssen, A. V. Ustinov, H. Kohlstedt, J. G. Caputo, S. Pagano, and N. Flytzanis, in *Proceedings of the International Conference on Nonlinear Superconducting Devices and High-Tc Materials*, edited by R. D. Parmentier and N. F. Pedersen (World Scientific, Singapore, 1994).

[21] Y. M. Ivanchenko, Phys. Rev. B **52**, 79 (1995).

[22] R. G. Mints and I. B. Snapiro, Phys. Rev. B **51**, 3054 (1995).

[23] R. G. Mints and I. B. Snapiro, Phys. Rev. B **52**, 9691 (1995).

[24] Y. E. Kuzvovlev and A. I. Lomtev, JETP **84**, 986 (1997).

[25] A. I. Lomtev, JETP **86**, 1234 (1998).

[26] J. G. Caputo, N. Flytzanis, V. V. Kurin, N. Lazarides, and E. Vavalis, J. Appl. Phys. **85**, 7282 (1999).

[27] N. Flytzanis, N. Lazarides, A. Chiginev, V. V. Kurin, and J. G. Caputo, J. Appl. Phys **88**, 4201 (2000).

[28] V. G. Kogan, V. V. Dobrovitski, J. R. Clem, Y. Mawatari, and R. G. Mints, Phys. Rev. B **63**, 144501 (2001).

[29] N. Grønbech-Jensen and M. R. Samuelsen, Phys. Rev. B **65**, 144512 (2002).

[30] J. Pearl, Appl. Phys. Lett. **5**, 65 (1964).

[31] G. J. Dolan, Appl. Phys. Lett. **31**, 337 (1977).

[32] M. Abramowitz and A. Stegun, eds., *Handbook of Mathematical Functions with Formulas, Graphs, and Mathematical Tables* (U.S. GPO, Washington, D.C., 1965).

[33] H. Hilgenkamp and J. Mannhart, Rev. Mod. Phys. **74**, 485 (2002).

[34] I. O. Kulik, JETP Lett. **2**, 84 (1965).

[35] I. O. Kulik, Sov. Phys. Tech. Phys. **12**, 111 (1967).

[36] A. A. Abdumalikov, Jr., and V. V. Kurin (unpublished).

[37] G. L. Lamb, *Elements of soliton theory* (Wiley, New York, 1980).

[38] N. Martucciello and R. Monaco, Phys. Rev. B **53**, 3471 (1996).